Heralded entanglement for quantum enhanced measurement with photons

Jonathan C. F. Matthews,* Alberto Politi,* Damien Bonneau, and Jeremy L. O'Brien[†]

Centre for Quantum Photonics, H. H. Wills Physics Laboratory & Department of Electrical and Electronic Engineering, University of Bristol, Merchant Venturers Building, Woodland Road, Bristol, BS8 1UB, UK

Generating quantum entanglement is not only an important scientific endeavour, but will be essential to realising the tremendous potential of quantum-enhanced technologies, in particular quantum-enhanced measurements with precision beyond classical limits. We report the heralded generation of multi-photon entanglement for quantum metrology using a reconfigurable integrated waveguide device in which projective measurement of auxiliary photons heralds the generation of path entangled states. From four and six photon inputs we heralded two- and four-photon "NOON" states—a superposition of N photons in two paths, which enable phase supersensitive measurements at the Heisenberg limit. Realistic devices will include imperfections and we demonstrate phase super-resolution with a state that is robust to photon loss. These results can be generalised to generate arbitrarily large entangled states of light for quantum metrology in an integrated optics architecture.

Quantum information science [1] promises secure communication [2], tremendous computational power [3] and the ultimate precision in measurement [4]. These technologies rely on encoding information in physical systems that exhibit the uniquely quantum mechanical properties of superposition and entanglement. Photons play a central role in the development of quantum science [5–8] and are attractive for quantum technologies [2, 9]. Photons offer low noise, ease of manipulation, high speed transmission; and entangling interactions between photons can be achieved using only linear optical circuits [10, 11]. To achieve these non-linear entangling interactions additional photons and photon detection can be used: a particular detection event heralds the success of a given process. In this way it is possible to generate multi-photon entangled states and indeed to efficiently perform universal, fault tolerant quantum computing [10]. There have been several examples of heralding multi-photon states in this way for various applications (*eg.* Refs. 12–17). Generating path entangled states, including NOON states, for quantum metrology is a particularly important example, where an N-photon entangled state is heralded from $> N$ input photons and several schemes for doing this have been proposed [18, 19].

Sub-wavelength sensitivity makes optical interferometry one of the most powerful precision measurement tools available to modern science and technology [20], with applications from microscopy to gravity wave detection [21, 22]. However, the use of classical states of light limits the phase precision $\Delta\phi$ of such measurements to the shot noise, or standard quantum limit (SQL): $\Delta\phi \cong 1/\sqrt{N}$, where N is the average number of photons used. Quantum states of light—entangled states of photon number across the two paths of the interferometer for example—enable precision better than the SQL [4]. Entangled states of $M + N$ photons across two optical modes x and y of the form

$$|N :: M\rangle_{x,y}^{\phi} = \tfrac{1}{\sqrt{2}}(|N\rangle_x |M\rangle_y + e^{i\phi} |M\rangle_x |N\rangle_y) \quad (1)$$

can be used to increase the frequency of interference fringes by a factor of $|N - M|$ and thereby increase preci-

sion. The canonical example is the NOON state ($M = 0$), which enables the ultimate precision $\Delta\phi \cong 1/N$—the Heisenberg limit [23]. While NOON states are fragile with respect to photon loss, other linear superpositions of photon number entanglement can beat the SQL in interferometers with loss: states with $M \neq N$ are optimal for balanced loss [24]. Realistic application of these entangled states, however, demands a scalable and practical means of generating large $|N :: M\rangle$ states.

Multi-photon interference, surpassing the SQL in some cases, has been observed with post-selected two-[25] three- [26] and four-photon states[27, 28], and with two-photon loss-tolerant non-maximally entangled states [29]. However, to benefit from the comparatively non-invasive properties of quantum metrology requires either a deterministic [30, 31] or a heralded [32, 33] method for generating high fidelity, large photon number $|N :: M\rangle_{x,y}^{\phi}$ states. For most precision measurement applications it is also important that the entangled state be encoded in two spatial modes (rather than polarization modes). Stability required for such encoding can be readily achieved in compact integrated quantum photonic devices [34, 35], as demonstrated by two-[36, 37] and four-photon [36] interference.

The silica-on-silcon waveguide device shown in Fig. 5(a) is capable of heralding the two- and four-photon NOON states $|2 :: 0\rangle_{j,k}^{0}$ and $|4 :: 0\rangle_{j,k}^{\pi}$, as well as the four-photon state $|3 :: 1\rangle_{j,k}^{0}$, dependent upon the input state and the setting of the internal phase ϕ, as we now explain. The circuit consists of directional couplers DC_{1-4}, equivalent to beam splitters, used to couple photons between optical modes and for quantum interference. The resistive heating element controls the relative optical phase ϕ inside the device. The state $|2 :: 0\rangle_{j,k}^{0}$ can be achieved by inputting four non-degenerate photons, via polarization maintaining fibre (PMF), in the (unentangled) state $|2\rangle_b |2\rangle_c$. Quantum interference at the first directional coupler DC_1—designed to have a reflectivity $\eta = 0.5$—generates a superposition of the components $|4\rangle_e |0\rangle_f$, $|2\rangle_e |2\rangle_f$ and $|0\rangle_e |4\rangle_f$. After DC_3 and DC_4 this state evolves to a superposition across the four modes i, g, h
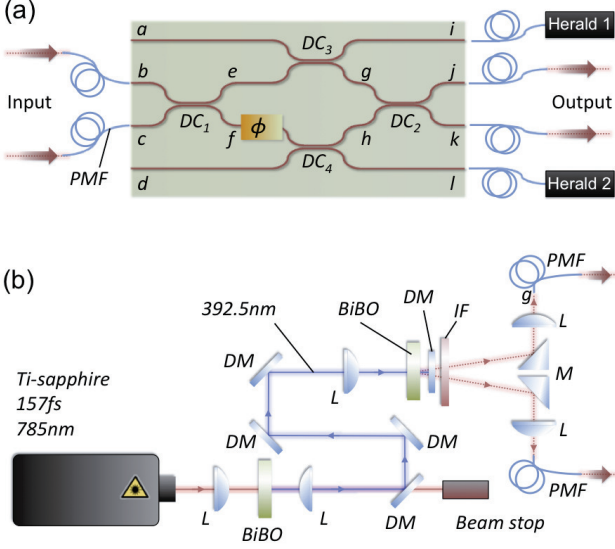
FIG. 1: Heralding multi-photon path-entangled states in a photonic chip. (a) The waveguide circuit with coupling reflectivities $DC_{1,2} = 1/2$, $DC_{3,4} = 1/3$. (b) Schematic of the pulsed down conversion source used to generate four- and six-photon (unentangled) states.
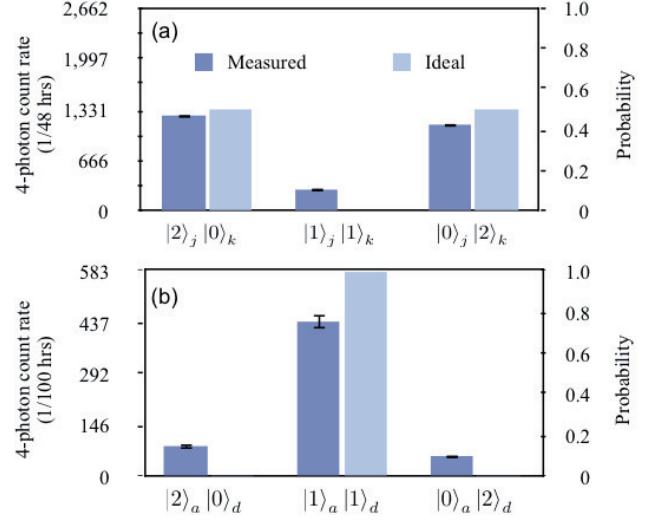

FIG. 2: Heralded $|20\rangle + |02\rangle$ state. (a) Measurement of photon statistics of the heralded two-photon NOON state. (b) Testing coherence of the heralded two-photon NOON state by measuring the photon statistics after non-classical interference at DC_2 via a fibre Sagnac loop. Both distributions are normalised using single photon detection rates to account for relative detector scheme, source and waveguide coupling efficiencies. Error bars are calculated from modelling the detection rates with Poissonian statistics.

and l. However, only the component $|2\rangle_e |2\rangle_f$ gives rise to terms that include $|1\rangle_i |1\rangle_l$. Detecting a single photon in these two heralding modes therefore projects the quantum state across modes g and h to $|1\rangle_g |1\rangle_h$. Quantum interference [38] at the final directional coupler DC_2 yields the two photon state $|2 :: 0\rangle_{j,k}^0$. Provided DC_3 and DC_4 are $\eta = 0.5$, the intrinsic success rate, *i.e.* the probability of detecting $|1\rangle_i |1\rangle_l$ and thereby heralding $|2 :: 0\rangle_{j,k}^0$, is 1/16 (Ref. 18, see Appendix). Note that the heralding of the $|1\rangle_i |1\rangle_l$ component eliminates the lower order state $|1\rangle_b |1\rangle_c$.

The four-photon states $|3 :: 1\rangle_{j,k}^\phi$ and $|4 :: 0\rangle_{j,k}^\pi$ are heralded in a similar manner: On inputting the state $|3\rangle_b |3\rangle_c$ into the chip, non-classical interference at DC_1 yields a coherent superposition of the components $|6\rangle_e |0\rangle_f$, $|4\rangle_e |2\rangle_f$, $|2\rangle_e |4\rangle_f$ and $|0\rangle_e |6\rangle_f$. On detecting one photon in each of the two modes i and l (again via DC_3 and DC_4) projects the state into a superposition state $|3 :: 1\rangle_{g,h}^\phi$. With the phase set to $\phi = 0$, the state returns to $|3 :: 1\rangle_{j,k}^0$ after DC_2. With the phase set to $\phi = \pi/2$, however, quantum interference at DC_2 yields the four photon NOON state $|4 :: 0\rangle_{j,k}^{\pi/2}$. For $\eta = 0.5$ for both DC_3 and DC_4, the success rate of heralding $|4 :: 0\rangle_{j,k}^\pi$ at the output is 3/64 (Ref. 18, see Appendix). Detection of the state $|4\rangle_j |0\rangle_k$ leads to an interference fringe as a function of ϕ, with resolution double that of classical light, providing an important means of testing quantum coherence within the optical circuit.

Four- and six-photon input states were generated using the setup shown in Fig. 5(b). Pulsed $\lambda = 785$ nm light

from a 157 fs, 80 MHz mode-locked Titanium:Sapphire laser system was up converted using a 2 mm nonlinear bismuth borate BiB_3O_6 (BiBO) crystal; the resulting $\lambda = 392.5$ nm light is separated from remaining infrared light using four dichroic mirrors (DM) and focused (L) to seed type-I spontaneous parametric downconversion in a second BiBO crystal. The photons created in this process pass through a high transmission interference filter (IF) with FWHM = 2.5 nm and are collected by focusing two points on opposite sides of the down conversion cone onto PMFs which are butt-coupled to the waveguide chip. Detection of multiple photon states in the same optical mode is accomplished non-deterministically using cascaded non-number resolving, optical fibre-coupled SPCMs (see Appendix).

The photon number statistics measured from the heralded two-photon NOON state at outputs j and k is plotted in Fig. 2(a). Fidelity between the measured probability distribution and the expected distribution for the ideal state $|2 :: 0\rangle_{j,k}^0$ (also plotted) is $F_i = 0.95 \pm 0.01$. For $\lambda = 785$nm operation, the reflectivities of DC_1 and DC_2 are measured to be $\eta = 0.542$ and 0.530 respectively. Using these measured reflectivities, the expected output state was simulated and comparison with experimental results yield a fidelity of $F_s = 0.96 \pm 0.01$, leaving the discrepancy with perfect fidelity attributed to six- and higher photon number terms from the down conversion process and residual distinguishability of photons and not the device itself.
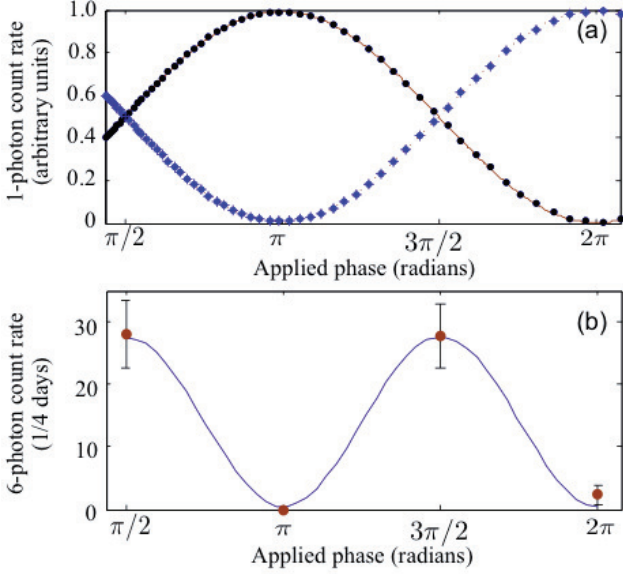
FIG. 3: Super resolution with a heralded four photon entangled state. (a) Single photon fringes from inputting light into waveguide b and varying the phase ϕ, displaying the expected pattern arising from classical interference pattern with period 2π. Black circles and blue diamonds respectively represent the normalised single photons count rate detected at output j and k. (b) The increased resolution interference fringe of manipulating ϕ of the state $|3::1\rangle_{e,f}^{\phi}$ with period π. The four data points represent six-photon count rates integrated over four days and normalized using single-photon count rates to account for coupling efficiency over time. Error bars are modelled from assuming Possonian statistics on the rate of detection. Blue sinusoidal plot of near unit contrast is plotted as a guide.

To test the coherence of the output of the circuit we formed a Sagnac loop by joining two optical fibres coupled to modes j and k (see Appendix). This configuration keeps relative optical phase of these modes fixed by the inherently stable Sagnac interferometer and results in quantum interference at DC_2 in the reverse direction. By coupling detectors to waveguides a and d, the photon statistics of the quantum state returning through the chip after DC_2 at g and h can be measured, with an intrinsic loss due to $DC_{3,4}$. The fidelity between the measured distribution (Fig. 2(b)) and the one expected from a perfect $|2::0\rangle_{j,k}^{0}$ state interfering at directional coupler DC_2 is $F_i = 0.90 \pm 0.03$. (Taking into account only the measured reflectivities of DC_1 and DC_2 the expected detection rates (not plotted) agree with the experimental measurements with fidelity $F_s = 0.97 \pm 0.03$.) This high fidelity demonstrates the coherence of the $|2::0\rangle_{e,f}$ state.

Although Fig. 2(b) demonstrates coherence of the output state, the four photon process that generates it does not rely on phase stability within the interferometer structure of the device. In contrast heralding the $|4::0\rangle_{j,k}^{0}$ state from the six photon input state $|3\rangle_b |3\rangle_c$ requires coherent generation of the state $|3::1\rangle_{g,h}^{0}$ within
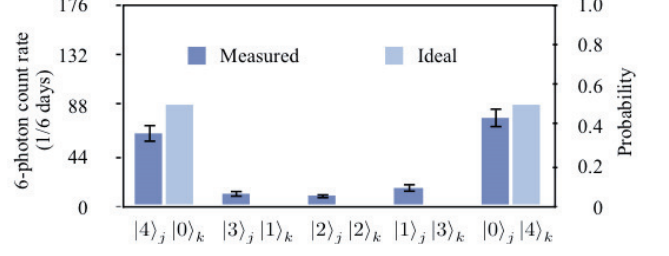

FIG. 4: Heralded generation of the $|40\rangle + |04\rangle$ state. The distribution of photon statistics from measuring a heralded four-photon NOON state. The six-fold detection rates are normalized by single photon detection rates to account for relative source, coupling and detection scheme efficiencies. Error bars are computed from modelling photon counts using Poissonian statistics.

the interferometer. To test this coherence we injected the state $|3\rangle_b |3\rangle_c$ into the chip and varied the phase ϕ. We observed the super-resolution interference pattern plotted in Fig. 3(b) via detection six photons in the state $|1\rangle_i |4\rangle_j |0\rangle_k |1\rangle_l$. As well as demonstrating coherence of the $|3::1\rangle_{g,h}^{0}$ state for subsequent generation of the $|4::0\rangle_{j,k}^{0}$ state, the data in 3b are a demonstration of phase super-resolution with a heralded state that is robust to loss, which will be crucial in real-world applications where imperfections are inevitable.

Fig. 4 shows the photon statistics of the $|4::0\rangle_{j,k}^{0}$ state that results from the quantum interference of the $|3::1\rangle_{g,h}^{\pi/2}$ at DC_2. We fixed the phase within the chip to $\phi = \pi/2$ and again injected the six-photon state $|3\rangle_b |3\rangle_c$ into the chip. Six photons were detected in all the possible four-photon combinations on outputs j and k, together with a single photon in each of the heralding modes i and l. The fidelity between the resulting distribution of photon statistics and the distribution expected from measuring the ideal state $|4::0\rangle_{j,k}^{0}$ is $F_i = 0.89 \pm 0.04$. Taking into account the measured reflectivities of DC_1 and DC_2, the expected statistics agree with experimental measurements with a fidelity $F_s = 0.93 \pm 0.04$. The remaining discrepancy is attributed to eight- and higher-photon number states and distinguishability of the photons generated in the down conversion process (see Appendix).

The heralded generation of path entangled states will be crucial to practical application of quantum metrology; the schemes presented here are scalable to arbitrary large entangled states [32]. States that are robust to loss will be particularly important. The integrated waveguide architecture delivers the high stability and compact implementation required for real world applications. In particular, integrated variable beam splitters [36] will allow optimisation of quantum state engineering in presence of loss [24]. The ongoing development of efficient detectors and deterministic photon sources such as single emitters or multiplexed down-conversion schemes[9], shows

promise for practical quantum metrology and other photonic quantum technologies when combined with circuits such as that described here. Future development will also require integration of fast feed-forward—using for example electro-optic materials—with the circuit demonstrated here to form a building block for scalable generation of arbitrarily large entangled states [32].

APPENDIX

Input State Evolution

The integrated circuit described in our Letter creates different quantum states depending on the input and on the value of the variable internal phase. Here we describe the evolution of the state for the inputs $|2\rangle_b |2\rangle_c$ and $|3\rangle_b |3\rangle_c$. Each directional coupler DC_i of reflectivity η_i acting on two optical paths is modelled with the matrix

$$DC_i \doteq \begin{pmatrix} \sqrt{\eta_i} & i\sqrt{1-\eta_i} \\ i\sqrt{1-\eta_i} & \sqrt{\eta_i} \end{pmatrix} \qquad (2)$$

with the assumption that coupler reflectivity in the circuit (Fig. 1(a) of the main text) have the values $\eta_1 = \eta_2 = 1/2$ and $\eta_3 = \eta_4 = 1/3$.

When the state $|2\rangle_b |2\rangle_c$ is launched into the device, the directional coupler DC_1 transforms the state to

$$|2\rangle_b |2\rangle_c \overset{DC_1}{\rightarrow} \sqrt{\frac{3}{4}} |4::0\rangle^0_{e,f} + \frac{1}{\sqrt{4}} |2\rangle_e |2\rangle_f . \qquad (3)$$

The couplers DC_3 and DC_4, combined with the subsequent detection of only one photon each in waveguides i and l, then project the state to

$$\sqrt{\frac{4}{81}} |1\rangle_i |1\rangle_g |1\rangle_h |1\rangle_l . \qquad (4)$$

The value of the variable phase ϕ is uninfluential in this case, since it can be treated as a global phase. Finally, this state non-classically interfers at directional coupler DC_2 to give the output

$$\sqrt{\frac{4}{81}} |1\rangle_i |2::0\rangle^0_{j,k} |1\rangle_l , \qquad (5)$$

corresponding to the two-photon NOON state $|2::0\rangle_{j,k}$ at the output of the photonic chip.

Similarly, when the state $|3\rangle_b |3\rangle_c$ is launched into the photonic circuit, non-classical interference at DC_1 transforms the state according to

$$|3\rangle_b |3\rangle_c \overset{DC_1}{\rightarrow} \sqrt{\frac{5}{8}} |6::0\rangle^0_{e,f} + \sqrt{\frac{3}{8}} |4::2\rangle^0_{e,f} . \qquad (6)$$

The couplers DC_3 and DC_4, combined with the subsequent detection of only one photon each in waveguides i and l, project the state to

$$|1\rangle_i \sqrt{\frac{4}{243}} \left(\frac{|3\rangle_g |1\rangle_h + e^{2i\phi} |1\rangle_g |3\rangle_h}{\sqrt{2}} \right) |1\rangle_l . \qquad (7)$$

The state $|3::1\rangle^0_{j,k}$ is created inside the photonic circuit after couplers DC_3 and DC_4. The variable internal phase ϕ (controllable via thermo-optical electrode) can be used to control this state, with the effect of non-classical interference at directional coupler DC_2 depending on the phase ϕ according to

$$|1\rangle_i \left(\sin\phi \sqrt{\frac{3}{64}} |4::0\rangle^\pi_{j,k} - \cos\phi \sqrt{\frac{3}{64}} |3::1\rangle^0_{j,k} \right) |1\rangle_l . (8)$$

It is noted that the internal phase ϕ is useful for two important tasks: confirming the quantum nature of the states inside the photonic chip, allowing the measurement of fringes with double the frequency of the one photon case reported in Fig. 3 of the main text; and for producing the desired state $|4::0\rangle_{j,k}$ at the output of the chip–as shown in Fig. 4 in the main text–with the choice $\phi = \pi/2$.

Detection Scheme

Here we show in detail the schemes used to detect multi-photon states at the output of the integrated chip. The detectors used are silicon avalanche single photon counting modules (SPCM) that do not discriminate photon number–the presence of one of more photons at the SPCM produces the same output electrical signal. To reconstruct multi-photon states, number resolution is needed, which can be obtained probabilistically when using multiple SPCM and optical splitters. Three splitters and four detectors were used to detect up to four photons in the same optical mode as shown in the scheme in Fig. 5(a). The splitters used are multi-mode fiber couplers, with a near-unity transmissivity and close to 50:50 splitting ratio. If we assume perfect detectors and 50:50 splitters, the probability of detecting four photons in the same optical mode with the above method is given by $1/4^4 \times 4! = 3/32$. Similarly, the probability of detecting three photons in one mode and one in the other is $1/4^4 \times 3! = 3/128$, and the probability of detecting two photons in two modes is $1/4^4 \times 2! = 3/256$. All multiphoton coincidental detection reported in the Letter are normalized to the appropriate detection probability using single counts recorded in each detector; this normalizes the multi-photon coincidental detections, taking into account deviations from perfect and uniform detectors, differences in transmissivity and splitting ratio of the couplers.

Fig. 5(b) illustrates the detection scheme used to test coherence of the nominally $|2::0\rangle_{j,k}$ state. The measurement of the state at the end of the chip featured in Fig. 2
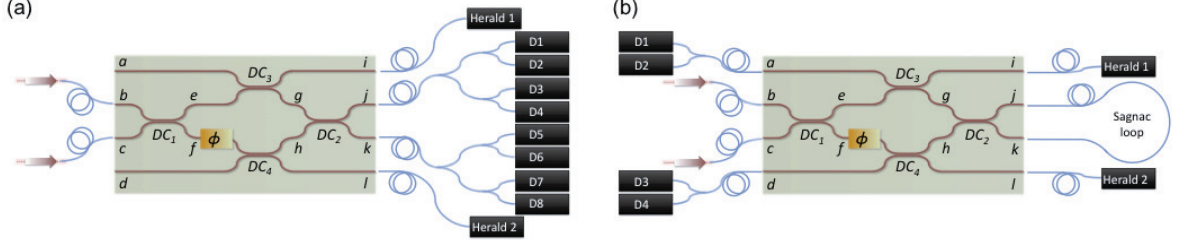
FIG. 5: Experimental setup for multi-photon state detection. (a) The detection scheme for detecting the six-photon state $|1\rangle_i |4::0\rangle_{j,k}^{\pi/2} |1\rangle_l$ at the output of the integrated chip. (b) The detection scheme for testing coherence of the nominally two-photon NOON state $|1\rangle_i |2::0\rangle_{j,k} |1\rangle_l$.

of the main text proves only that the state is mainly composed mainly by the components $|20\rangle_{j,k}$ and $|02\rangle_{j,k}$ but gives no information about the purity of the state. The coherence of the output state can be confirmed by interfering the photons in the paths j and k at a further directional coupler, since the result of this action is different in the case of a pure or a mixed state. This further interference cannot be achieved outside the integrated chip, otherwise the phase stability required for the experiment would be lost. We obtain non-classical interference at directional coupler DC_2, after the state is coupled out and back in the integrated chip via a fibre Sagnac loop between waveguides j and k, ensuring complete phase stability of the photonic state; any variation in path registered by photons traveling from waveguide j to k is experienced also by photons traveling from waveguide k to j. The photons are then probabilistically extracted from the chip via the directional couplers DC_3 and DC_4 and detected with cascaded detectors as for the other measurements.

The multi-photon detection coincidences were registered and elaborated with a in-house FPGA virtex-4 board electronic circuit. The circuit works in the following way as illustrated on Fig. 6(a). When a channel receives a pulse from the detector, the rising edge of the pulse is converted in an internal pulse synchronised with the FPGA clock. Such signal is then used to detect coincidences. We define an internal coincidence window T_{IC} which is a multiple of the clock cycle T_{Clk}. If two or more synchronised signals from different channels fall within the window, then a coincidence is recorded for those events. Since the FPGA clock is not synchronised with the detector, the effective coincidence window does not have a rectangular shape as shown on Fig. 6(b). In fact the probability to detect a coincidence is 100% when the delay T_{Delay} between the first and the last pulse is bellow $T_{IC} - T_{Clk}$. Then the probability to detect a coincidence falls linearly as T_{Delay} increases from $T_{IC} - T_{Clk}$ to T_{IC}, with no coincidence detected when the delay is increased further. For this experiment, to account for the overall jitter of the six SPCM, we chose $T_{IC} = 3T_{Clk}$ while the clock cycle of the FPGA is

$T_{Clk} \approx 2.9ns$. The counting logic has been checked using a Quantum Composer Plus 5218. We measured an 100% efficiency detection window of 6ns and no detection after a delay of 9ns.

Higher Photon Number Contributions

The photonic input needed for the 6-photon experiment to produce the states $|3::1\rangle_{j,k}^{0}$ and $|4::0\rangle_{j,k}^{\pi/2}$ corresponds to the state $|3\rangle_b |3\rangle_c$. Experimentally, an approximation of this state can be created via parametric down conversion, and it can be written as

$$|\psi\rangle_{bc} \sim |00\rangle + \xi |11\rangle + \xi^2 |22\rangle + \xi^3 |33\rangle + \xi^4 |44\rangle + ... \quad (9)$$

As described in the text, the $|00\rangle$ and $|11\rangle$ states are rejected by detection of two heralding photons. For the six photon experiments other components with a number of total photons lower than six (i.e. $|22\rangle$) have no effect, since they cannot give rise to six-photon simultaneous events. On the other hand, the input component with eight photons can give a recordable event, since losses and detectors without photon number resolution wash out the information about the input state.

The effect of the state $|4\rangle_b |4\rangle_c$ acting as an input of the integrated chip is analyzed here. Non-classical interference at DC_1 transforms the state to

$$|4\rangle_b |4\rangle_c \overset{DC_1}{\to} \frac{\sqrt{35}}{8} |8::0\rangle_{e,f}^{0} + \frac{\sqrt{5}}{4} |6::2\rangle_{e,f}^{0} + \frac{3}{8} |4\rangle_e |4\rangle_f \quad (10)$$

To understand what happens if the eight-photon term is present in the circuit in the configuration adopted in this experiment, it should be noted that eight photons can give rise to six-photon coincidental detection in different ways. Since the general analysis is rather complex, we limit here to the case of $\phi = \pi/2$. For this phase, the complete state that can give rise to allowed events is of
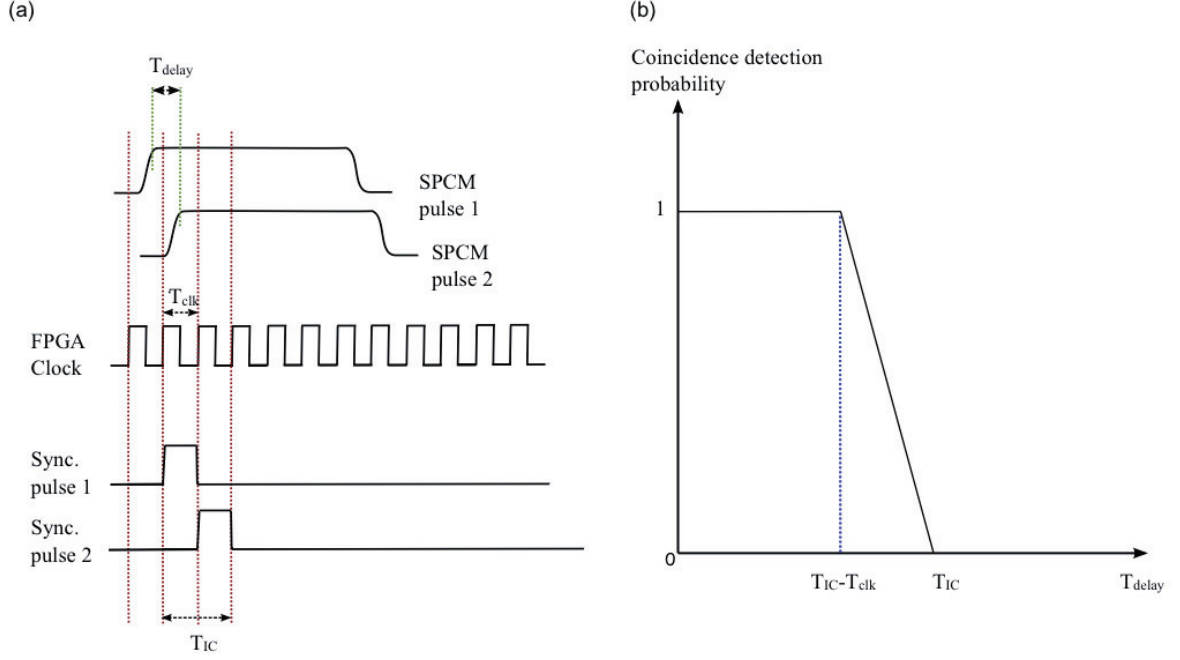
FIG. 6: (a) An example of detection of coincidence for two channels 1 and 2. From the pulses of the detector SPCM pulse 1 (respspectively SPCM pulse 2), the synchronised signals Sync. pulse 1 (Sync pulse 2) are generated. A coincidence is then detected when two signals fall within T_{IC}. (b) The probability to detect a coincidence as a function of the delay between the two pulses.

the form

$$
\frac{i\sqrt{2}}{162} |1\rangle_i \left(3\sqrt{5} |6::0\rangle_{j,k}^0 - \sqrt{3} |4::2\rangle_{j,k}^0 \right) |1\rangle_l
$$

$$
+ \frac{\sqrt{2}}{54\sqrt{3}} |2\rangle_i \left(-3\sqrt{5} |5::0\rangle_{j,k}^{-\pi/2} - i |4::1\rangle_{j,k}^{\pi/2} \right.
$$

$$
\left. + \sqrt{2} |3::2\rangle_{j,k}^{-\pi/2} \right) |1\rangle_l
$$

$$
+ \frac{\sqrt{2}}{54\sqrt{3}} |1\rangle_i \left(3i\sqrt{5} |5::0\rangle_{j,k}^{\pi/2} + |4::1\rangle_{j,k}^{-\pi/2} \right.
$$

$$
\left. - i\sqrt{2} |3::2\rangle_{j,k}^{\pi/2} \right) |2\rangle_l
$$

$$
+ \frac{2}{162} |2\rangle_i \left(-7\sqrt{3} |4::0\rangle_{j,k}^0 + 3 |2\rangle_j |2\rangle_k \right) |2\rangle_l \quad (11)
$$

It is clear that the eight-photon input term can give rise to a quite complex pattern of detection. In particular, all the terms apart from the first of each row can give rise to detection of the $|3::1\rangle_{j,k}$ and $|22\rangle_{j,k}$ state.

To minimize the effect of the higher order emission of the BiBO down-conversion crystal, the value of ξ was chosen to be $\xi \sim 0.085$, that corresponds to a power of the blue beam pumping the down-conversion crystal of $P_b = 215$ mW. This choice of ξ is a good compromise between the six-photon detection rate and the unwanted production of eight photons. This is confirmed by Fig. 4 of the main text, since the count rates for the states $|3::1\rangle_{j,k}$ and $|22\rangle_{j,k}$ is low in comparison to the $|4::0\rangle_{j,k}$ term. To obtain higher quality states a true $|3\rangle_b |3\rangle_c$ could be be used. The generation of these Fock-

states is in principle possible. Although being a complex problem, Fock states can be generated using different methods, for example linear optics [39] or atom-cavity systems [40].

* These authors contributed equally
† Electronic address: Jeremy.OBrien@bristol.ac.uk

[1] M. A. Nielsen and I. L. Chuang, *Quantum Computation and Quantum Information* (Cambridge University Press, 2000).
[2] N. Gisin and R. Thew, Nature Photon. **1**, 165 (2007).
[3] T. D. Ladd, F. Jelezko, R. Laflamme, Y. Nakamura, C. Monroe, and J. L. OBrien, Nature **464**, 45 (2010).
[4] V. Giovannetti, S. Lloyd, and L. Maccone, Science **306**, 1330 (2004).
[5] S. J. Freedman and J. F. Clauser, Phys. Rev. Lett. **28**, 938 (1972).
[6] A. Aspect, P. Grangier, and G. Roger, Physical Review Letters **47**, 460 (1981).
[7] J.-W. Pan, D. Bouwmeester, M. Daniell, H. Weinfurter, and A. Zeilinger1, Nature **403**, 515 (2000).
[8] D. Bouwmeester, J. W. Pan, K. Mattle, M. Eibl, H. Weinfurter, and A. Zeilinger, Nature **390**, 575 (1997).
[9] J. L. O'Brien, A. Furusawa, and J. Vučković, Nature Photon. **3**, 687 (2009).
[10] E. Knill, R. Laflamme, and G. J. Milburn, Nature **409**, 46 (2001).
[11] J. L. O'Brien, Science **318**, 1567 (2007).
[12] S. Gasparoni, J.-W. Pan, P. Walther, T. Rudolph, and

A. Zeilinger, Phys. Rev. Lett. **93**, 020504 (2004).

[13] R. Okamoto, J. L. O'Brien, H. F. Hofmann, T. Nagata, K. Sasaki, and S. Takeuchi, Science **323**, 483 (2009).

[14] X.-H. Bao, T.-Y. Chen, Q. Zhang, J. Yang, H. Zhang, T. Yang, and J.-W. Pan, Phys. Rev. Lett. **98**, 170502 (2007).

[15] Q. Zhang, X.-H. Bao, C.-Y. Lu, X.-Q. Zhou, T. Yang, T. Rudolph, and J.-W. Pan, Phys. Rev. A **77**, 062316 (2008).

[16] R. Prevedel, G. Cronenberg, M. S. Tame, M. Paternostro, P. Walther, M. S. Kim, and A. Zeilinger, Phys. Rev. Lett. **103**, 020503 (2009).

[17] W. Wieczorek, R. Krischek, N. Kiesel, P. Michelberger, G. Tóth, and H. Weinfurter, Phys. Rev. Lett. **103**, 020504 (2009).

[18] H. Lee, P. Kok, N. J. Cerf, and J. P. Dowling, Phys. Rev. A **65**, 030101 (2002).

[19] J. Fiurášek, Phys. Rev. A **65**, 053818 (2002).

[20] F. Mayinger and O. Feldmann, *Optical Measurements: Techniques and Applications, 2nd edn* (Springer, 2002).

[21] A. Abramovici, W. E. Althouse, R. W. P. Drever, Y. Gursel, S. Kawamura, F. J. Raab, D. Shoemaker, L. Sievers, R. E. Spero, K. S. Thorne, et al., Science **256**, 325 (1992).

[22] K. Goda, O. Miyakawa, E. E. Mikhailov, S. Saraf, R. Adhikari, K. McKenzie, R. Ward, S. Vass, A. J. Weinstein, and N. Mavalvala, Nature Physics **4**, 472 (2008).

[23] J. P. Dowling, Contemp. Phys. **49**, 125 (2008).

[24] R. Demkowicz-Dobrzanski, U. Dorner, B. J. Smith, J. S. Lundeen, W. Wasilewski, K. Banaszek, and I. A. Walmsley, Phys. Rev. A **80**, 013825 (2009).

[25] Z. Y. Ou, X. Y. Zou, L. J. Wang, and L. Mandel, Phys. Rev. A **42**, 2957 (1990).

[26] M. W. Mitchell, J. S. Lundeen, and A. M. Steinberg, Nature **429**, 161 (2004).

[27] P. Walther, J. W. Pan, M. Aspelmeyer, R. Ursin, S. Gasparoni, and A. Zeilinger, Nature **429**, 158 (2004).

[28] T. Nagata, R. Okamoto, J. L. O'brien, K. Sasaki, and S. Takeuchi, Science **316**, 726 (2007).

[29] M. Kacprowicz, R. Demkowicz-Dobrzanski, W. Wasilewski, K. Banaszek, and I. A. Walmsley (????), URL arXiv.org:0906.3511.

[30] H. F. Hofmann and T. Ono, Phys. Rev. A **76**, 031806 (2007).

[31] A. Afek, O. Ambar, and Y. Silberberg, arXiv:0912.4009v2 [quant-ph] (2009).

[32] H. Cable and J. P. Dowling, Phys. Rev. Lett. **99**, 163604 (2007).

[33] H. Kim, H. S. Park, and S.-K. Choi, Optics Express **17**, 19720 (2009).

[34] A. Politi, M. J. Cryan, J. G. Rarity, S. Yu, and J. L. O'Brien, Science **320**, 646 (2008).

[35] G. D. Marshall, A. Politi, J. C. F. Matthews, P. Dekker, M. Ams, M. J. Withford, and J. L. O'Brien, Opt. Express **17**, 12546 (2009).

[36] J. C. F. Matthews, A. Politi, A. Stefanov, and J. L. O'Brien, Nat. Photonics **3**, 346 (2009).

[37] B. J. Smith, D. Kundys, N. Thomas-Peter, P. G. R. Smith, and I. A. Walmsley, Opt. Express **17**, 13516 (2009).

[38] C. K. Hong, Z. Y. Ou, and L. Mandel, Phys. Rev. Lett. **59**, 2044 (1987).

[39] Sanaka, K. *Phys. Rev. A* **71**, 021801 (2005).

[40] Brattke, S., Varcoe, B. T. H. & Walther, H. *Phys. Rev. Lett.* **86**, 3534 (2001).